Clim. Past Discuss., 9, 75–118, 2013
www.clim-past-discuss.net/9/75/2013/
doi:10.5194/cpd-9-75-2013

Climate of the Past Discussions

Mid-Holocene ocean and vegetation feedbacks over East Asia

Z. Tian[1,2] **and D. Jiang**[1,3,4]

[1]Nansen-Zhu International Research Centre, Institute of Atmospheric Physics, Chinese Academy of Sciences, Beijing, China
[2]University of Chinese Academy of Sciences, Beijing, China
[3]Key Laboratory of Regional Climate-Environment Research for Temperate East Asia, Chinese Academy of Sciences, Beijing, China
[4]Climate Change Research Center, Chinese Academy of Sciences, Beijing, China

Received: 6 November 2012 – Accepted: 20 December 2012 – Published: 4 January 2013

Correspondence to: Z. Tian (tianzhiping@mail.iap.ac.cn)

Published by Copernicus Publications on behalf of the European Geosciences Union.

Abstract

Mid-Holocene ocean and vegetation feedbacks over East Asia were investigated by a set of numerical experiments performed with the latest version 4 of the Community Climate System Model (CCSM4). Most of the annual and seasonal surface air temperature and precipitation changes during the mid-Holocene relative to the pre-industrial period were found to result from a direct response of the atmosphere to insolation forcing, while dynamic ocean and vegetation could modulate regional climate over East Asia to a certain extent. Because of its thermal inertia, the dynamic ocean induced an additional warming (cooling) of 0.5 K in boreal winter, 0.0003 K in boreal summer, and 1.0 K in boreal autumn (0.6 K in boreal spring) averaged across China during the mid-Holocene, and hence counteracted (amplified) the direct response except in summer, collectively leading to a weak annual warming of 0.2 K at the national scale. The contribution of dynamic vegetation to mid-Holocene temperature change was small overall. It gave rise to an additional annual cooling of 0.2 K, 0.1 K in winter, 0.2 K in summer, and 0.4 K in autumn, but a warming of 0.1 K in spring regionally averaged over China. On the other hand, ocean feedback led to a small enhancement of precipitation by 0.04 mm day^{-1} in winter and 0.05 mm day^{-1} in autumn, but induced a reduction of precipitation by 0.14 mm day^{-1} for the annual mean, 0.29 mm day^{-1} in spring, and 0.34 mm day^{-1} in summer at the national scale, which tended to weaken East Asian summer monsoon rainfall. The influence of dynamic vegetation on precipitation was comparatively small, with a regionally averaged precipitation change of –0.002 mm day^{-1} on the annual scale, –0.03 mm day^{-1} in winter and spring, –0.01 mm day^{-1} in summer, and 0.06 mm day^{-1} in autumn over the country. Taken together, ocean feedback narrowed the model–data mismatch in annual and winter temperatures over China during the mid-Holocene, while dynamic vegetation feedback contributed little to temperature and precipitation changes over East Asia.

CPD
9, 75–118, 2013

1 Introduction

Paleoclimate modeling is one of the most important aspects in past climate change research. Combining model results with proxy data provides a unique opportunity to investigate the cause and effect of natural variability of past climate over a range of timescales, which is of significance when trying to better understand the present climate, as well as predict and project future climate changes.

The mid-Holocene is a period that occurred approximately 6000 yr before present, when the climate and environment were significantly different from today due to a change in incoming solar radiation at the top of the atmosphere (Berger, 1978). It is an ideal time period for studying past climate change on the orbital scale, during which paleoclimatic proxy records are abundant and relatively reliable. The mid-Holocene is also one of the key benchmark periods under the protocol of the Paleoclimate Modeling Intercomparison Project (PMIP), with its initial stage (PMIP1) designed to test the atmospheric component of climate models (atmospheric general circulation models: AGCMs) and its second and third stages (PMIP2 and PMIP3) having incorporated the roles of the dynamic ocean (atmosphere–ocean general circulation models: AOGCMs) and vegetation (atmosphere–ocean–vegetation general circulation models: AOVGCMs). The impact of the variability in the Earth's orbital parameters on mid-Holocene climate has been intensively studied through a number of paleoclimate simulations (e.g. Joussaume et al., 1999; Braconnot et al., 2000, 2007; Liu et al., 2004; Wohlfahrt et al., 2004; Otto et al., 2009a, b; O'ishi and Abe-Ouchi, 2011; Zhao and Harrison, 2012). These studies have shown that, although insolation changes were the primary cause of mid-Holocene climate change, interactive ocean and vegetation, as well as their synergy effects, might also have considerably modified the annual and seasonal climate response to mid-Holocene insolation. However, there is no consensus on the relative magnitude of such feedback mechanisms, the strength of the synergy between them, and the degree to which the expression of the response to ocean and vegetation feedbacks varied regionally. Besides, previous studies have focused mainly

CPD
9, 75–118, 2013

on mid-Holocene climate change either at the global scale or over the monsoon regions of northern or southern Africa, North or South America, or northern Australia, and less attention has been paid to East Asian monsoon regions. Thus, more extensive modeling of mid-Holocene climate change, as well as the roles of ocean and vegetation feedbacks and their synergy, both at global and regional scales, appears to be necessary.

Considerable effort has been devoted to reconstructing mid-Holocene climate over East Asia using a variety of proxy data, which has demonstrated that China experienced warmer and wetter than present conditions as a whole during that time (see Sect. 5). In contrast to the abundant proxy data, very little paleoclimate modeling work has been carried out for the East Asian region. Only a few simulations of East Asian climate during the mid-Holocene have been performed using AGCMs (Wang, 1999, 2000, 2002; Chen et al., 2002), regional climate models nested within AGCMs (Zheng et al., 2004; Liu et al., 2010), and synchronously- or asynchronously-coupled AOGCMs (Wei and Wang, 2004; Zheng and Yu, 2009). In those earlier studies, warmer-than-present climate and intensified monsoon circulation over East Asia during the mid-Holocene summer (June–August) have been reproduced well, but the geographical distribution and magnitude of summer climate change have varied among simulations, indicative of a large degree of uncertainty in this region. In addition, less attention has been paid to features of the annual mean, or indeed the three seasons other than summer. Therefore, it is important to examine what East Asian climate was like during the mid-Holocene in simulations by state-of-the-art climate models. Second, both positive (e.g. Braconnot et al., 2000; Wei and Wang, 2004; Zhao and Harrison, 2012) and negative (e.g. Liu et al., 2004; Ohgaito and Abe-Ouchi, 2007; Li and Harrison, 2008; Marzin and Braconnot, 2009) effects of interactive ocean on mid-Holocene Asian monsoon precipitation have been shown in previous studies. It is of interest to examine this issue further using current climate models. Third, dynamic vegetation feedback was typically ignored in most of previous simulations of East Asian climate during that period. Recently, Jiang et al. (2012) found that 35 of (all) the 36 PMIP1 and PMIP2

CPD
9, 75–118, 2013

models reproduced colder-than-baseline annual (winter, December–February) temperatures over China during the mid-Holocene, which are in stark contrast to warmer-than-present conditions as derived from multiple proxy data sources. In addition, they also showed that ocean–atmosphere interaction induced a warming effect on annual, winter, and autumn (September–November) temperatures, while vegetation–atmosphere interaction had little impact on annual and seasonal temperatures. However, the differences between the AGCM and AOGCM (AOGCM and AOVGCM) control simulations in the PMIP models introduced a bias into the role of ocean–atmosphere (vegetation–atmosphere) interaction in mid-Holocene climate change. Therefore, another key purpose of this study is to examine pure ocean and vegetation feedbacks for East Asian climate during the mid-Holocene using rigorous experiments based on one of the latest coupled atmosphere–ocean–vegetation climate models.

After a short description of the model and experimental design in Sect. 2, we discuss the simulated climate change over East Asia between the mid-Holocene and pre-industrial period (Sect. 3). The contributions of ocean and vegetation feedbacks are further examined in Sect. 4. Finally, following a model–data comparison in Sect. 5, a discussion and conclusions are presented in Sect. 6.

2 Methods

2.1 Model and experiments

The National Center for Atmospheric Research (NCAR) Community Climate System Model version 4 (CCSM4) is a globally coupled ocean–atmosphere–sea-ice–land-surface climate model. A detailed description of the model can be found in Gent et al. (2011), and the following is a brief outline of the four model components. The atmospheric model is the NCAR Community Atmosphere Model version 4 (CAM4; Neale et al., 2010), which employs a T31 spectral dynamical core at a horizontal resolution of approximately 3.75° × 3.75° and with 26 vertical levels. The land model, run on

CPD
9, 75–118, 2013

the same horizontal grid as the atmosphere, is the Community Land Model version 4 (CLM4; Lawrence et al., 2012). Based on the Parallel Ocean Program (POP) of the Los Alamos National Laboratory (Smith et al., 2010), the ocean model component (POP2) is described in Danabasoglu et al. (2012), which uses the nominal 3° horizontal gird with 60 levels in the vertical direction. The sea ice component is based on the Community Ice Code version 4 (CICE4; Hunke and Lipscomb, 2008), and major updates of the ice model compared to CCSM3 are discussed in Holland et al. (2012). The ice model uses the same horizontal grid as the ocean model component. Further details on CCSM4 are available at http://www.cesm.ucar.edu/models/ccsm4.0/, and information on the model improvements and specifics about the higher resolution simulations can be found in Gent et al. (2011) and Shields et al. (2012).

CCSM4, with the same low horizontal resolution of T31, has been tested against observation and reanalysis data to evaluate its performance in reproducing present day East Asian climate (Tian et al., 2012), and the results showed a reliable capability for doing so in terms of large-scale climate features over East Asia and China. Specifically, the model captured well the spatial pattern of surface air temperature and precipitation over China, sea level pressure, geopotential height at 500 hPa and 100 hPa, and the wind field at 850 hPa over East Asia, although the magnitudes differed somewhat from observations.

The experiments were designed to separate the contribution of ocean and vegetation feedbacks from total climate change between the mid-Holocene (6-ka) and pre-industrial (0-ka) period. The boundary conditions for the 0-ka and 6-ka experiments are listed in Table 1. The major difference between the experiments for the two periods was the Earth's orbital parameters derived from Berger (1978), which led to an increase in the seasonal cycle of incoming solar radiation at the top of the atmosphere in the Northern Hemisphere and a decrease in the Southern Hemisphere. The 6-ka simulation under the PMIP3 protocol also considered a reduction in atmospheric CH_4 concentration from 791.6 ppbv to 650 ppbv, a small atmospheric CO_2 concentration reduction from 284.5 ppmv to 280 ppmv, and N_2O from 275.7 ppbv to 270 ppbv.

CPD
9, 75–118, 2013

Altogether, six experiments were undertaken, as listed in Table 2. We first performed two sets of experiments with the fully coupled CCSM4: a pre-industrial control simulation with 0-ka orbital parameters and atmospheric concentrations of greenhouse gases (GHGs; AOV(0 ka)), and a mid-Holocene simulation with 6-ka orbital parameters and GHGs (AOV(6 ka)) following the control run and 6-ka experiment of PMIP3. To spin up the AOV(0 ka) experiment, we first ran the carbon–nitrogen (CN) model to a steady state, which was started with an initial condition of no vegetation using the "accelerated decomposition spinup" mode for 651 model years. Then, we continued from the end of this simulation and ran the carbon–nitrogen dynamic global vegetation (CNDV) model for 200 more years. After that, we used the last state from the CNDV spinup as initial conditions to run the fully coupled AOV(0 ka) experiment for a further 800 yr until the vegetation distribution reached equilibrium. Taken together, the AOV(0 ka) simulation was run for 1651 model years. In AOV(6 ka), the model was continued from the last state of AOV(0 ka) and ran for 400 yr until the global vegetation pattern showed an equilibrium state. Second, we performed two AOGCM simulations without dynamic vegetation. In the pre-industrial and mid-Holocene simulations with "fixed vegetation" (AO(0 ka) and AO(6 ka)), the vegetation was prescribed at the pre-industrial equilibrium state from AOV(0 ka). These two AOGCMs were run for 800 yr and 700 yr, respectively, until they were in near surface equilibrium, with trends in global surface air temperature being less than 0.05 °C century^{-1} (Braconnot et al., 2007). In order to analyze the contribution of ocean–atmosphere interaction, we performed two additional atmosphere-only runs (A(0 ka) and A(6 ka)) with "fixed vegetation" from AOV(0 ka) and "fixed SSTs" from the pre-industrial equilibrium state in AO(0 ka). Both of the AGCM simulations were run for 30 yr. The output from the last 100 model years in the two AOVGCM and two AOGCM simulations, and the last 20 yr in the two AGCM simulations, were used for the following analysis.

CPD
9, 75–118, 2013

2.2 Analysis methods

As described above, the present AOGCM and AGCM simulations shared the same vegetation as in the AOVGCM 0-ka simulation, and the AGCM simulations shared the same SSTs as in the AOGCM 0-ka simulation, as suggested by Braconnot et al. (2007), Dallmeyer et al. (2010), O'ishi and Abe-Ouchi (2011), and Jiang et al. (2012). In this sense, dynamic vegetation feedback could be directly measured by (AOV(6 ka)–AOV(0 ka))–(AO(6 ka)–AO(0 ka)), and the dynamic ocean feedback by (AO(6 ka)–AO(0 ka))–(A(6 ka)–A(0 ka)).

In order to quantitatively examine the extent to which the performance of this single model over East Asia matches those of other models, we also compared the present simulation results to all 35 available PMIP coupled experiments at this stage, including 14 AOGCMs plus six AOVGCMs from PMIP2 and eight AOGCMs plus seven AOVGCMs from PMIP3. Detailed information about the above PMIP models and experimental designs are available online at http://pmip2.lsce.ipsl.fr/ and http://pmip3.lsce.ipsl.fr/. Note that the coupled atmosphere–ocean model CCSM4 with fixed vegetation as in the pre-industrial simulation at a higher resolution, roughly $0.9^{\circ} \times 1.25^{\circ}$ (hereafter referred to as CCSM4-f09), participated in the PMIP3, which differs from our low resolution version of CCSM4 (hereafter referred to as CCSM4-T31) with dynamic vegetation.

3 Mid Holocene East Asian climate change

Before discussing the effects of dynamic ocean and vegetation feedbacks (next section), here we first describe the large-scale climate changes between 6-ka and 0-ka over East Asia based on the fully coupled experiments AOV(6 ka) and AOV(0 ka). In our analysis we focus on surface air temperature (temperature at 2 m above ground), effective precipitation, and East Asian summer monsoon.

CPD
9, 75–118, 2013

3.1 Surface air temperature

Figure 1 shows the geographical distribution of annual and seasonal surface temperature changes over East Asia between 6-ka and 0-ka. Under the framework of the PMIP experiments, the annual mean incoming insolation was reduced by 0.36 W m^{-2} averaged over China during the mid-Holocene relative to the present day (Berger, 1978). Following the above insolation change, the East Asian region experienced an annual cooling ranging from 0 K to 1.5 K at 6-ka, apart from in the area north of 50° N. The surface air temperature decrease over China was less than 1 K, and the temperature change over Northeast China was less obvious (< 0.2 K). The differences of regionally averaged annual and seasonal temperatures over China between 6-ka and 0-ka in our experiments and the 35 PMIP coupled models are jointly shown in Fig. 2. Averaged across the whole country, annual temperature was reduced by 0.5 K at 6-ka with respect to 0-ka in our simulation, which was within the national cooling magnitudes in 12 of the 13 PMIP AOVGCMs ranging from –0.7 K to –0.0 K, but contrary to the warming of 0.3 K in the HadGEM2-ES model.

According to the algorithm of Berger (1978), the regionally averaged insolation over China at 6-ka was reduced by 10.97 W m^{-2} in winter, 8.20 W m^{-2} in spring (March–May), and 3.62 W m^{-2} in autumn, but increased by 21.34 W m^{-2} in summer with respect to 0-ka. Similar to the annual mean, seasonal temperature change also closely followed the above insolation change over China at 6-ka. Cooler (warmer) than 0-ka surface air temperature was reproduced over most parts of China in winter and spring (in summer), with temperature change averaged by –1.3 K and –1.5 K (1.1 K) over China, respectively, which was within the range of the 13 PMIP AOVGCMs (Fig. 2). In autumn, the temperature change amplitude during the mid-Holocene was overall less than that in the other seasons, with a weak cooling of 0.1 K averaged over China. This autumn cooling was mainly induced by the insolation reduction during that time, though it was inconsistent with the warming effects nationally averaged from 0.2 K to 0.8 K in 12 of the

CPD
9, 75–118, 2013

13 PMIP AOVGCMs (Fig. 2). By contrast, the FGOALS-s2 model reproduced a similar amplitude of autumn cooling at the national scale as in our simulation result.

3.2 Precipitation, evaporation and effective precipitation

The annual and seasonal changes for effective precipitation, i.e. the difference between precipitation and evaporation (P–E), between 6-ka and 0-ka are illustrated in Fig. 3. The overall magnitude of precipitation changes over East Asia was about 2–3 times larger than that for evaporation (figures not shown). Figure 4 also shows the percentage change of regionally averaged precipitation over China during the mid-Holocene with respect to the baseline climate in our experiments and from 24 of the 35 PMIP models, which were selected for their ability to reproduce the modern climatology of precipitation over China (Jiang et al., 2013).

On the annual scale, mid-Holocene precipitation increased by 0.1 mm day^{-1} to 0.5 mm day^{-1} over the Qinghai-Tibetan Plateau, Inner Mongolia, Northeast China, and most parts of India, but reduced by 0.1 mm day^{-1} to 0.5 mm day^{-1} over the middle and lower reaches of the Yangtze River valley and the East China Sea. At the national scale, precipitation reduced by 0.05 mm day^{-1} over China during the mid-Holocene, which was a 1.7% decrease with respect to 0-ka. On the other hand, evaporation increased slightly by 0.02 mm day^{-1} to 0.2 mm day^{-1} over most parts of China and northern India. On average, annual effective precipitation change was similar to that of precipitation both in spatial pattern and magnitude. By contrast, when seen from the 10 PMIP AOVGCMs, three (seven) models showed a reduction (an enhancement) of annual precipitation during the mid-Holocene, with regionally averaged changes ranging from –1.0 % to –0.4 % (2.3 % to 7.4 %) over China relative to 0-ka (Fig. 4), which was weaker than (opposite to) our simulation result.

The mid-Holocene precipitation reduction, regionally averaged by –0.16 mm day^{-1} in winter and –0.40 mm day^{-1} in spring over China, was larger in magnitude than that of evaporation, leading to a deficit of effective precipitation over most parts of China in those two seasons. With respect to 0-ka, winter (spring) precipitation decreased by

CPD
9, 75–118, 2013

5.7 % (14.3 %) averaged across China, within (beyond) the range of the changes in the 10 PMIP AOVGCMs nationally averaged from –15.1 % to –2.8 % (–12.4 % to 1.8 %) (Fig. 4). The geographical distributions of summer precipitation, evaporation, and effective precipitation change at 6-ka over China were similar to those for the annual mean, with the change magnitudes in the former larger than in the latter. In autumn, effective precipitation change during the mid-Holocene was less than 1 mm day^{-1} over East Asia. Averaged across China, summer and autumn precipitation was increased by 7.4 % and 5.9 % relative to 0-ka, respectively, within the range obtained from the 10 PMIP AOVGCMs in summer and nine AOVGCMs in autumn (Fig. 4).

3.3 East Asian summer monsoon

The East Asian summer monsoon (EASM) features southerly winds over East China and western branches of the western North Pacific subtropical high from June to August in the lower troposphere. In response to an increase of ∼5 % in the seasonal insolation distribution in the Northern Hemisphere (Berger, 1978), the EASM had been inferred to intensify during the mid-Holocene based on previous experiments of individual AOGCMs (Chen et al., 2002; Marzin and Braconnot, 2009; Zhou and Zhao, 2009; Liu et al., 2010; Bosmans et al., 2012) and some of the PMIP models (Wang et al., 2010; Zhao and Harrison, 2012). It is suggested that an enhanced land–sea thermal contrast, and hence sea level pressure gradient between the East Asian continent and the adjacent oceans, was responsible for the EASM strengthening during the mid-Holocene.

As shown in Fig. 5, obvious southwesterly wind anomalies were present over South and East China, and further northward to Japan and the Korean Peninsula, which corresponded to significantly stronger EASM at 6-ka than at 0-ka. As a result, the southerly wind anomalies favored increased water vapor from the South China Sea to the continent of East Asia, leading to an increase in the mid-Holocene summer precipitation over South China, as well as over the Korean Peninsula and Japan (Fig. 3). The easterly wind anomalies, which originated from southern branches of the anomalous

CPD
9, 75–118, 2013

anticyclone over the Okhotsk Sea, provided abundant water vapor from the western North Pacific to Northeast China, contributing to increased summer precipitation over that region. Of note is that summer monsoon precipitation during the mid-Holocene was reduced over the middle and lower reaches of the Yangtze River valley, which was opposite to the result in Wang et al. (2010). This might be because there were no obvious easterly wind anomalies at 850 hPa over the adjacent oceans, and hence less water vapor could be transported from the western North Pacific to supplement the water vapor from the South China Sea, which could hardly transport further north and inland.

4 Mid-Holocene ocean and vegetation feedbacks over East Asia

In previous studies, analysis of dynamic ocean (vegetation) feedback during the mid-Holocene was not straightforward because AGCM and AOGCM (AOGCM and AOVGCM) experiments of mid-Holocene climate have used different control experiments. For example, a comparison between the two sets of simulations based on PMIP1 AGCMs and PMIP2 AOGCMs did not strictly diagnose the ocean feedback owing to different versions of the atmospheric component (Zhao and Harrison, 2012), which also introduced a bias between the SST-forced and the coupled control simulations as addressed by Marzin and Braconnot (2009). Furthermore, when investigating vegetation feedback, it is more reasonable to run the AOGCM 6-ka simulation with prescribed vegetation of the AOVGCM 0-ka simulation, as suggested by Braconnot et al. (2007), Dallmeyer et al. (2010), and O'ishi and Abe-Ouchi (2011). In the present study, the aforementioned biases were taken into account to obtain more realistic results. The AOGCM and AGCM 6-ka simulations shared the same 0-ka simulation (AO(0 ka)), while the AOVGCM and AOGCM experiments for 6-ka climate shared the same control experiment (AOV(0 ka)). Therefore, the difference between (AO(6 ka)–AO(0 ka)) and (A(6 ka)–A(0 ka)) allowed us to clearly discuss the role of

CPD
9, 75–118, 2013

ocean feedback, and the difference between (AOV(6 ka)–AOV(0 ka)) and (AO(6 ka)–AO(0 ka)) allowed us to examine the role of vegetation feedback during the mid-Holocene.

Before discussing the contribution of ocean and vegetation feedbacks, it was necessary to simply describe the direct response of the atmosphere to orbital forcing during the mid-Holocene (figures not shown), which was determined by the difference between A(6 ka) and A(0 ka). Following the orbital-induced insolation change over China between 6-ka and 0-ka, the direct response of the atmosphere was an annual cooling of 0.5 K, 1.8 K in winter, 1.0 K in spring, and 0.7 K in autumn, but a warming of 1.3 K in summer regionally averaged over China during the mid-Holocene, all of which were within the temperature change range of the 16 PMIP1 AGCMs as shown in Jiang et al. (2012). Precipitation increased on average by 0.09 mm day^{-1} for the annual mean, 0.56 mm day^{-1} in summer, and 0.06 mm day^{-1} in autumn, but reduced by 0.17 mm day^{-1} in winter and 0.09 mm day^{-1} in spring over the country during the mid-Holocene. These changes were generally consistent with the results of the 12 PMIP1 AGCMs as assessed by Jiang et al. (2013), apart from in summer.

4.1 Dynamic ocean feedback

The ocean was an important component of the climate system in the East Asian monsoon region during the mid-Holocene. Multiple modeling studies have indicated that ocean feedback plays a considerable role in mid-Holocene climate change. Several studies have reported that the ocean amplifies orbitally-induced changes in the northern African monsoon (e.g. Kutzbach and Liu, 1997; Hewitt and Mitchell, 1998; Braconnot et al., 2000; Voss and Mikolajewicz, 2001; Liu et al., 2004). Regarding the Asian monsoon, however, there is less consensus. Some simulations have shown an increase of Asian monsoon precipitation due to the effect of ocean–atmosphere interaction (e.g. Braconnot et al., 2000; Wei and Wang, 2004; Zhao and Harrison, 2012), while others have suggested a damping of Asian summer precipitation (e.g. Liu et al., 2004; Ohgaito and Abe-Ouchi, 2007; Li and Harrison, 2008; Marzin and Braconnot, 2009).

CPD
9, 75–118, 2013

These differences in Asian monsoon behavior provided the motivation to re-examine ocean feedback effects on East Asian climate change during the mid-Holocene using a state-of-the-art coupled climate model.

4.1.1 Surface air temperature

Owing to the large thermal inertia of the ocean, changes in sea surface temperature (SST) lag changes in insolation by about 1–2 months. The large-scale annual and seasonal SST changes between 6-ka and 0-ka shown in Fig. 6 were quite similar to those in the ensemble mean of the 10 PMIP3 models with SST outputs available (figures not shown). Figure 7 shows the annual and seasonal surface air temperature changes during the mid-Holocene due to ocean feedback. On average, annual SSTs increased north of 50° N but decreased to the south over the adjacent oceans of East Asia, which caused a weak temperature warming from 0.2 K to 0.5 K over most parts of China, but a small cooling over the other regions of East Asia during the mid-Holocene, though most of the changes were not robust at the 90 % confidence level. As shown in Fig. 2, ocean feedback induced an annual warming of 0.2 K averaged across China, which was close to the ocean-induced warming of 0.3 K obtained from the 22 PMIP AOGCMs and the aforementioned 16 PMIP1 AGCMs. As a whole, the contribution of ocean feedback to annual temperature change over China during the mid-Holocene partly counteracted the direct response of the atmosphere to orbital forcing.

Owing to higher SSTs over the adjacent oceans of the East Asian continent in autumn and their lag effect, ocean–atmosphere interaction led to a warming of surface temperature over almost all considered regions of East Asia in autumn and over most parts of China in winter during the mid-Holocene, which both counteracted the direct cooling response of the atmosphere to the insolation change in these two seasons. Note that the autumn warming was robust over most parts of China. The negative ocean feedback was consistent with the result over East Asian monsoon regions from Dallmeyer et al. (2010) in winter, but opposite to the positive effect in autumn therein. As shown in Fig. 2, winter (autumn) temperature increased regionally by 0.5 K (1.0 K) over

CPD
9, 75–118, 2013

China due to ocean feedback, with a similar magnitude (0.5 K) of nationally-averaged ocean-induced warming derived from the 22 PMIP AOGCMs and 16 PMIP1 AGCMs.

The colder-than-0-ka SSTs in the oceans adjacent to mainland China during mid-Holocene spring exerted a cooling effect from 0.2 K to 1.5 K over almost all considered areas of East Asia in spring, with the ocean-induced temperature change averaged by –0.6 K across China, thereby amplifying the direct insolation impact. In mid-Holocene summer, SSTs were higher than at 0-ka over the Japan Sea and areas north of 45° N, but colder over other oceans adjacent to the East Asian continent. As a result, surface air temperature increased by 0.2 K to 0.5 K over the region approximately between 34° N and 44° N in China, as well as over the Japan Sea and East India, but decreased by 0.2 K to 0.5 K over other regions of East Asia, contributing to a very weak ocean-induced summer warming of 0.0003 K averaged across China. The strong (very weak) positive ocean feedback in spring (summer) was generally consistent with (opposite to) the result over East Asian monsoon regions in Dallmeyer et al. (2010). Contrary to our model results, however, the ocean-induced temperature change was 0.03 K in spring and –0.04 K in summer at the national scale as obtained from the 22 PMIP AOGCMs and 16 PMIP1 AGCMs, which indicates an extent of uncertainty in the mid-Holocene ocean feedback among individual climate models.

4.1.2 Precipitation

The dynamic ocean influence on seasonal precipitation distributions is mainly revealed by the change of evaporation from the ocean and the alteration of large-scale and local circulations due to changed SSTs. Figure 8 (Fig. 9) illustrates the annual and seasonal sea-level pressure and 850 hPa wind (precipitation) changes due to ocean feedback during the mid-Holocene. Lower than 0-ka annual SSTs south of 50° N over the oceans adjacent to the East Asian continent reduced evaporation and weak high-pressure anomalies appeared over the western Pacific, which were accompanied by decreased water vapor transportation from the South China Sea to southern and eastern China (Fig. 8), resulting in a non-robust reduction of precipitation over those regions

CPD
9, 75–118, 2013

(Fig. 9). Averaged across China, ocean feedback induced a weak decrease of annual precipitation by 0.14 mm day^{-1} during the mid-Holocene, which balanced out the orbitally induced precipitation increase over China. However, with respect to 0-ka, regionally averaged annual precipitation over China was enhanced by 4.2 % at 6-ka in the ensemble mean of the 14 PMIP AOGCMs as shown in Fig. 4, which was greater than the enhancement of 2.5 % in the 12 PMIP1 AGCMs in Jiang et al. (2013), indicating an ocean-induced precipitation increase that disagreed with our model result.

Higher SSTs over the oceans adjacent to East Asia in autumn and the lag effect in winter increased evaporation, and high-pressure anomalies occurred over the western Pacific in the former season and over the Japan Sea in the latter season (see Fig. 8). As a result, the accompanying increase in moist air advection from the ocean to the continent was responsible for the small enhancement of winter and autumn precipitation over a large part of China during the mid-Holocene (Fig. 9). Averaged across China, precipitation increased by 0.04 mm day^{-1} (0.05 mm day^{-1}) in winter (autumn) due to ocean feedback, and partly compensated (amplified) the atmospheric response to the insolation change. In mid-Holocene spring and summer, lower-than-0-ka SSTs over the adjacent oceans of mainland China and large-scale circulation anomalies led to a reduction of precipitation over most parts of China in these two seasons. The most remarkable change in summer precipitation occurred over East China, with the strongest reduction reaching 3 mm day^{-1}. At the national scale, the ocean-induced precipitation decrease was averaged by 0.29 mm day^{-1} in spring and 0.34 mm day^{-1} in summer during the mid-Holocene, thereby amplifying the direct atmospheric effect in spring but counteracting the direct response in summer.

As obtained from the 14 PMIP AOGCMs and the aforementioned 12 PMIP1 AGCMs, ocean–atmosphere interaction led to a country-averaged reduction (enhancement) of precipitation both in spring and winter (in autumn and summer) over China, which was consistent with our model result in the former season but inconsistent in the latter. In addition, the positive ocean feedback for the spring precipitation decrease in the present study was also in line with that over the Yangtze and Huanghe plain (31.54°–38.97° N,

CPD
9, 75–118, 2013

105°–120° E) as discussed in Dallmeyer et al. (2010). However, the negative ocean feedback for the summer precipitation change over China at 6-ka indicated a weakening of East Asian summer monsoon rainfall, which was also revealed by Dallmeyer et al. (2010) and in agreement with the conclusions drawn by Liu et al. (2004), Ohgaito and Abe-Ouchi (2007), Li and Harrison (2008), and Marzin and Braconnot (2009), but in disagreement with the studies of Braconnot et al. (2000), Wei and Wang (2004), and Zhao and Harrison (2012).

4.2 Dynamic vegetation feedback

Vegetation feedback has been proposed as an important process contributing to the mid-Holocene climate system (Jansen et al., 2007). Previous simulations have shown that changes in vegetation during the mid-Holocene modified and amplified the climate system response to an enhanced seasonal cycle of insolation in the Northern Hemisphere both directly, primarily through changes in surface albedo, and indirectly through changes in SSTs, sea-ice extent, ocean circulation, and so on (Ganopolski et al., 1998). Studies concerning the impact of vegetation feedback on mid-Holocene climate change have mostly focused on the African monsoon region (e.g. Kutzbach et al., 1996; Braconnot et al., 1999; Levis et al., 2004), as well as the Asian monsoon region (e.g. Wang, 1999; Texier et al., 2000; Diffenbaugh and Sloan, 2002; Li et al., 2009). Vegetation effect has been investigated through both reconstructed paleovegetation (e.g. Chen et al., 2002; Zheng et al., 2004; Liu et al., 2010) and dynamic vegetation modules (e.g. Gallimore et al., 2005; Dallmeyer et al., 2010; O'ishi and Abe-Ouchi, 2011), which could induce an overall warming of annual temperature over China during the mid-Holocene. Recently, Jiang et al. (2012) found that vegetation–atmosphere interaction had little impact on annual and seasonal temperatures over China according to six pairs of the PMIP2 models with and without vegetation effects. However, the AOGCM and AOVGCM experiments of the 6-ka climate therein did not share the same or similar 0-ka experiments, which introduced a bias into the effect of vegetation–atmosphere interaction over China at 6-ka.

CPD
9, 75–118, 2013

In order to evaluate mid-Holocene vegetation feedback over East Asia more clearly, we re-examined the role of dynamic vegetation in climate change during the mid-Holocene with strict experimental designs using the latest version of the coupled model CCSM4, the higher resolution version of which participated in the PMIP3. From our simulation results, the vegetation change over East Asia between 6-ka and 0-ka was very small (figures not shown). Thus, we could not expect a large effect of vegetation feedback over that region compared to those of orbital forcing and ocean feedback.

4.2.1 Surface air temperature

The annual and seasonal temperature changes between 6-ka and 0-ka due to vegetation feedback are shown in Fig. 10. We can see clearly from the color scales that the average contribution of dynamic vegetation to mid-Holocene temperature change was relatively small. On the annual scale, most parts of China experienced a cooling from 0.1 K to 0.5 K, while part of Northeast China, the southern Qinghai-Tibetan Plateau and southwestern China underwent a weak warming from 0.1 K to 0.3 K due to vegetation feedback at 6-ka. Averaged across the whole country, the effect of dynamic vegetation induced an annual cooling of 0.2 K, amplifying the direct atmospheric response during the mid-Holocene. As inferred from Fig. 2, the positive vegetation feedback was consistent with the result from the pair of FOAM models showing a vegetation-induced cooling of 0.4 K, but opposite to the warming effect of 0.06 K in the ensemble mean of the 13 AOVGCMs as compared to the ensemble mean of the 22 AOGCMs in the PMIP.

In winter, mid-Holocene temperature decreased by 0.3 K to 1 K due to vegetation feedback over a large part of China apart from Northeast China and the Qinghai-Tibetan Plateau. On the one hand, Northeast China is covered by snow in winter, such that the increased forest fraction at 6-ka could give rise to a higher snow-masking effect and a decrease in surface albedo, resulting in a robust increase of surface temperature by up to 1 K. On the other hand, the Qinghai-Tibetan Plateau experienced an additional winter warming of around 0.5 K. During the mid-Holocene, vegetation feedback gave rise to an additional cooling north of 30° N over East Asia in summer

CPD
9, 75–118, 2013

and over the whole region of East Asia except for only two grid-boxes in autumn, with the robust cooling over China occurring both over northern Xinjiang and part of North China. The temperature decrease was probably concerned with an increase in cloudiness and evapotranspirational cooling of the surface resulted from an enlargement of the forest fraction area in those two seasons. By contrast, South China experienced a weak vegetation-induced summer warming from 0.1 K to 0.3 K at 6-ka. Averaged across China, vegetation feedback led to an additional cooling of 0.1 K in winter, 0.2 K in summer, and 0.4 K in autumn during the mid-Holocene. However, most parts of China showed a weak warming from 0.1 K to 0.5 K in spring due to vegetation feedback, with a regionally averaged value of 0.1 K at the national scale. The small increase in spring forest was accompanied by a reduced surface albedo and a warming of the atmosphere due to more absorbed shortwave radiation at the surface. Additionally, strong snow-melt albedo feedback also contributed to the spring warming.

Averaged across the 13 AOVGCMs and 22 AOGCMs in the PMIP as shown in Fig. 2, interactive vegetation induced a warming (cooling) effect of 0.08 K in winter and 0.17 K in autumn (0.02 K in spring and 0.01 K in summer) at the national scale in China, both of which were opposite to our model result (apart from in summer). In spite of the above inconsistencies, vegetation feedback for seasonal temperature changes during the mid-Holocene did agree with that in some pairs of the PMIP2 models as shown in Jiang et al. (2012), such as the winter and autumn cooling effects in the pairs of FOAM models, and the spring warming and summer cooling effects in the pairs of MRI-CGCM2.3.4fa models. Similar vegetation-induced warming in spring could further be obtained from the ensemble mean of the six pairs of PMIP2 models, and could also be seen over the Yangtze and Huanghe plain as indicated by Dallmeyer et al. (2010). However, these authors showed a robust warming of 0.16 K in autumn over the Qinghai-Tibetan Plateau, and 0.22 K in winter over the Yangtze and Huanghe plain due to interactive vegetation effects, both of which disagreed with the present simulations. Collectively, there were large differences, both in sign and magnitude, in the vegetation-induced annual and seasonal temperature changes during the mid-Holocene among

CPD
9, 75–118, 2013

our simulation, some previous experiments, and the latest PMIP model results, which indicates a degree of uncertainty.

4.2.2 Precipitation

Mid-Holocene annual and seasonal precipitation was affected very little by dynamic vegetation feedback, and robust changes could not be detected in our experiments (Fig. 11). On average, annual precipitation decreased slightly over the southern Qinghai-Tibetan Plateau and southwestern China and increased over the rest of China, with the change magnitude no more than 0.2 mm day^{-1}. Averaged across the whole country, vegetation feedback induced a very weak decrease in annual precipitation by 0.002 mm day^{-1} during the mid-Holocene, consistent with the vegetation-induced precipitation change in the ensemble mean of the PMIP coupled models as inferred from Fig. 4. With respect to 0-ka, annual precipitation at 6-ka was enhanced by 3.0 % at the national scale in the ensemble mean of the 10 PMIP AOVGCMs, which was weaker than the enhancement of 4.2 % in the ensemble mean of the 14 AOGCMs.

On the seasonal scale, most parts of China experienced a small reduction of precipitation by 0.05 mm day^{-1} to 0.2 mm day^{-1} in winter and by 0.05 mm day^{-1} to 0.3 mm day^{-1} in spring during the mid-Holocene due to vegetation feedback. Conversely, precipitation increased slightly by 0.05 mm day^{-1} to 0.2 mm day^{-1} both over a large part of the Qinghai-Tibetan Plateau in winter and over Northeast and Southwest China in spring. As a result, vegetation feedback led to a weak reduction of winter and spring precipitation, both by around 0.03 K, averaged across China at 6-ka. In summer, mid-Holocene precipitation decreased by 0.1 mm day^{-1} to 0.5 mm day^{-1} over most parts of the Qinghai-Tibetan Plateau and Southwest China, whereas it increased by 0.05 mm day^{-1} to 0.5 mm day^{-1} over the rest of China due to vegetation feedback, contributing to a small reduction of precipitation by 0.01 mm day^{-1} at the national scale. By contrast, autumn precipitation enhanced by 0.05 mm day^{-1} to 0.5 mm day^{-1} over a large part of China due to vegetation feedback, apart from the northern part of Northeast China, with an increase in precipitation by 0.06 mm day^{-1} averaged over the country.

CPD
9, 75–118, 2013

This effect could be attributed to the fact that, in autumn during the mid-Holocene, larger areas of China were covered by forest than in the pre-industrial period, when grass and desert were prevalent, resulting in increased evapotranspiration due to the greater leaf area, and thus more local precipitation.

As demonstrated by comparing the ensemble means of the 10 AOVGCMs and 14 AOGCMs in the PMIP, vegetation feedback led to an enhancement of precipitation in winter and spring but a reduction in summer and autumn during the mid-Holocene, among which only the summer precipitation decrease was consistent in sign with our model result. Similarly, no robust vegetation-induced seasonal precipitation changes were found over the East Asian monsoon regions as indicated by Dallmeyer et al. (2010). It is worth mentioning that most parts of India also experienced an enhancement of precipitation by 0.1 mm day^{-1} to 0.4 mm day^{-1} in autumn (Fig. 11). This was in accordance with the study by Dallmeyer et al. (2010), which showed that the vegetation-induced precipitation change in autumn was only robust over the Indian subcontinent, and increased regionally by 0.12 mm day^{-1} during the mid-Holocene.

5 Model–data comparison

Many efforts have been devoted to reconstructing the mid-Holocene climate over China by use of various proxy data. By collecting a number of "reliable" mid-Holocene temperature reconstructions over China, we chose the records of pollen, lake cores, paleosol, ice cores, peat, sediment, stalagmites, and fossil fruits at 64 sites (see Fig. 2 in Jiang et al., 2012) for model–data comparison purposes. These paleoenvironmental and paleoclimatic data indicate that stable, warmer-than-present climate conditions are prevalent over China during the mid-Holocene (Fig. 12). Specifically, annual temperature elevation was approximately 1 K over southern China, approximately 2 K over the Yangtze River valley, and 3 K over most parts of northern China. The strongest warming was recorded 4–5 K on the Qinghai-Tibetan Plateau. These records were in general consistent with the previous proxy data summarized by Shi et al. (1993). As assessed in Jiang et al. (2012), previous studies also indicate warmer-than-present winter

CPD
9, 75–118, 2013

temperatures during the mid-Holocene (e.g. Yu et al., 1998, 2000; Ni et al., 2010), and some studies further suggest that winter warming was stronger than the annual mean over China during that period (Xu et al., 1988; Kong et al., 1990, 1991; Shi et al., 1993; Tang et al., 2000; Guiot et al., 2008; Jiang et al., 2010; Wen et al., 2010).

Contrary to the annual and winter temperature warming as reconstructed by the aforementioned multiple proxy data sources, our model results reproduced colder-than-pre-industrial annual and winter climates during the mid-Holocene over the whole country, except for Northeast China where temperature change was not significant, with annual (winter) temperature decreasing regionally by 0.5 K (1.3 K) averaged across China in the AOVGCMs. Annual (winter) temperature cooling was also shown in 33 (all) of the 35 PMIP coupled models as seen in Fig. 2, with the nationally averaged temperature change ranging from –0.02 K to –1.0 K (–0.5 K to –2.0 K). Thus, both this study and the PMIP models show a considerable mismatch between the proxy data and simulations over China during the mid-Holocene. From the difference between the AOGCMs and AGCMs in our experiments, annual (winter) temperature increased by 0.2 K (0.5 K) averaged across China during the mid-Holocene due to ocean feedback, making the model results better agree with reconstructed records, which was also the case in the ensemble mean of the PMIP models. However, dynamic vegetation feedback in this study amplified the annual and winter temperature cooling, inducing an additional temperature decrease by 0.2 K and 0.1 K at the national scale, respectively. These results indicate that ocean feedback narrowed the model–data mismatch in annual and winter temperatures over China during the mid-Holocene, whereas vegetation feedback pushed the model further away from proxy data. In this sense, the impacts of dynamic ocean and vegetation on mid-Holocene temperature change over East Asia were of significant necessity to be taken into account.

For annual precipitation or humidity changes during the mid-Holocene, several reconstructed records are summarized in Wang et al. (2010), including lake cores, ice cores, peat, stalagmites, and fluvial profiles at 24 sites. According to the records, which covered a large part of China, mid-Holocene annual precipitation was greater in

CPD
9, 75–118, 2013

amount than at present, being 70–80 % higher in the Qianghai Lake area and showing a 30 % increase over Daihai Lake, Hidden Lake, and Ren Co Lake. Our model results were generally consistent with reconstructions over the latter three areas, but underestimated precipitation change in the Qinghai Lake area. In additon, the simulated precipitation reduction over central China disagreed with the reconstruction. However, records are very sparse over Northeast and East China, preventing model–data comparisons over those areas. Therefore, there is an urgent need for more reconstrutions with a larger coverage area and density for precipitation or humidity changes over China during the mid-Holocene.

6 Discussion and conclusion

The impacts of dynamic ocean and vegetation feedbacks on mid-Holocene climate change over East Asia were investigated by utilizing a new generation of the earth system model CCSM4. The strict experimental setup used in this study made it more straightforward and realistic to discuss ocean and vegetation feedbacks, with the AOGCM and AGCM simulations of mid-Holocene climate sharing the same control simulation and the AOVGCM and AOGCM 6-ka experiments sharing the same 0-ka experiment, as suggested by Braconnot et al. (2007), Dallmeyer et al. (2010), O'ishi and Abe-Ouchi (2011), and Jiang et al. (2012).

During the mid-Holocene, annual and seasonal surface air temperature changes over China in the fully coupled CCSM4 (AOVGCMs) resulted mainly from the imposed insolation forcing and the reduction of atmospheric concentrations of greenhouse gases, and the corresponding annual and winter cooling over China was contrary to the warming reconstructed from multiple proxy data, as shown in Shi et al. (1993), Yu et al. (2000), Ni et al. (2010), and Jiang et al. (2012). The simulated mid-Holocene annual effective precipitation over the Qinghai-Tibetan Plateau, Inner Mongolia, and Northeast China was greater in amount than pre-industrial levels, but less in amount over the middle and lower reaches of the Yangtze River valley, which was generally consistent with the reconstructed records as summarized by Wang et al. (2010) in the

CPD
9, 75–118, 2013

former regions but opposite to those in the latter regions. Taken together, the large-scale characteristics of East Asian climate change during the mid-Holocene were generally in accordance with previous studies (Braconnot et al., 2007; Dallmeyer et al., 2010; Jiang et al., 2012).

Under the background of a direct response of the atmosphere to orbital forcing, the dynamic ocean and vegetation feedbacks could modify the annual and seasonal temperature and precipitation changes during the mid-Holocene. As a whole, ocean feedback made the mid-Holocene annual and winter temperatures in the coupled model much closer to proxy data than those in the atmosphere-only model, as was the case obtained from the PMIP models. Ocean feedback also led to a weakened East Asian summer monsoon during the mid-Holocene. The average contribution of dynamic vegetation to mid-Holocene temperature changes over China was relatively small, and robust precipitation changes could not be detected. In addition, there were differences between our model results and the PMIP simulations in the effect of vegetation–atmosphere interaction on temperature and precipitation changes over China during the mid-Holocene, indicating a level of model-dependent uncertainty, which might partly arise from different experimental designs. Therefore, the spread of vegetation feedback during the mid-Holocene over East Asia implies a necessity for further investigation in terms of cause and effect.

The present model–data mismatch in annual and winter temperatures and annual precipitation over China during the mid-Holocene raises the question as to whether the inconsistency originates from the model, the proxy data, or both. It can be deduced from our analysis, as well as some previous studies (Dallmeyer et al., 2010; Jiang et al., 2012), that the incorporation of the dynamic ocean brings the annual and winter temperatures from the model and proxy data much closer together. However, a large degree of uncertainty, both in sign and magnitude, exists in the contribution of dynamic vegetation to mid-Holocene temperature and precipitation changes over China, as derived from the results in our simulation and the PMIP experiments. Additionally, the sparse spatial coverage of proxy data during the mid-Holocene, especially

CPD
9, 75–118, 2013

for precipitation or humidity changes, also indicates uncertainties of reconstructed warmer- and wetter-than-present climate over China during that time. Collectively, the improvement of earth system models as well as more reliable reconstruction work using multiple proxy datasets with extensive coverage are required to narrow the mismatch of model–data comparison over China.

Acknowledgements. We sincerely thank the National Center for Atmospheric Research (NCAR) for providing the CCSM4 model, the National Science Foundation (NSF) and the US Department of Energy (DOE) for sponsoring CCSM Project, and Joyce Bosmans, Pascale Braconnot, Johann Jungclaus, Akio Kitoh, Allegra N. LeGrande, Charline Marzin, Rumi Ohgaito, Bette L. Otto-Bliesner, Steven J. Phipps, Leon Rotstayn, Stéphane Sénési, Tongwen Wu, and Tianjun Zhou for information on the PMIP3 AOVGCMs and AOGCMs. Also, we acknowledge the international modeling groups for providing their data for analysis, and the Laboratoire des Sciences du Climat et de l'Environnement (LSCE) for collecting and archiving the PMIP model data. This research was supported by the Strategic Priority Research Program (XDA05120703 and XDB03020600) and the Knowledge Innovation Program (KZCX2-EW-QN202) of the Chinese Academy of Sciences and by the National Natural Science Foundation of China (41222034 and 41175072).

References

Berger, A.: Long-term variations of daily insolation and quaternary climatic changes, J. Atmos. Sci., 35, 2362–2367, 1978.

Bosmans, J. H. C., Drijfhout, S. S., Tuenter, E., Lourens, L. J., Hilgen, F. J., and Weber, S. L.: Monsoonal response to mid-holocene orbital forcing in a high resolution GCM, Clim. Past, 8, 723–740, doi:10.5194/cp-8-723-2012, 2012.

Braconnot, P., Joussaume, S., Marti, O., and Noblet, N. D.: Synergistic feedbacks from ocean and vegetation on the African monsoon response to mid-Holocene insolation, Geophys. Res. Lett., 26, 2481–2484, 1999.

Braconnot, P., Marti, O., Joussaume, S., and Leclainche, Y.: Ocean feedback in response to 6 kyr BP insolation, J. Climate, 13, 1537–1553, 2000.

Braconnot, P., Otto-Bliesner, B., Harrison, S., Joussaume, S., Peterchmitt, J.-Y., Abe-Ouchi, A., Crucifix, M., Driesschaert, E., Fichefet, Th., Hewitt, C. D., Kageyama, M., Kitoh, A., Laîné, A.,

CPD
9, 75–118, 2013

Loutre, M.-F., Marti, O., Merkel, U., Ramstein, G., Valdes, P., Weber, S. L., Yu, Y., and Zhao, Y.: Results of PMIP2 coupled simulations of the Mid-Holocene and Last Glacial Maximum – Part 1: experiments and large-scale features, Clim. Past, 3, 261–277, doi:10.5194/cp-3-261-2007, 2007.

Chen, X., Yu, G., and Liu, J.: Mid-Holocene climate simulation and discussion on the mechanism of temperature changes in eastern Asia, Sci. China Ser. D, 32, 335–345, 2002 (in Chinese).

Dallmeyer, A., Claussen, M., and Otto, J.: Contribution of oceanic and vegetation feedbacks to Holocene climate change in monsoonal Asia, Clim. Past, 6, 195–218, doi:10.5194/cp-6-195-2010, 2010.

Danabasoglu, G., Bates, S. C., Briegleb, B. P., Jayne, S. R., Jochum, M., Large, W. G., Peacock, S., and Yeager, S. G.: The CCSM4 ocean component, J. Climate, 25, 1361–1389, 2012.

Diffenbaugh, N. S. and Sloan, L. C.: Global climate sensitivity to land surface change: the mid holocene revisited, Geophys. Res. Lett., 29, 1476, doi:10.1029/2002GL014880, 2002.

Gallimore, R., Jacob, R., and Kutzbach, J.: Coupled atmosphere–ocean–vegetation simulations for modern and mid-Holocene climates: role of extratropical vegetation cover feedbacks, Clim. Dynam., 25, 755–776, 2005.

Ganopolski, A., Kubatzki, C., Claussen, M., Brovkin, V., and Petoukhov, V.: The influence of vegetation–atmosphere–ocean interaction on climate during the mid-Holocene, Science, 280, 1916–1919, 1998.

Gent, P. R., Danabasoglu, G., Donner, L. J., Holland, M. M., Hunke, E. C., Jayne, S. R., Lawrence, D. M., Neale, R. B., Rasch, P. J., Vertenstein, M., Worley, P. H., Yang, Z.-L., and Zhang, M.: The Community Climate System Model version 4, J. Climate, 24, 4973–4991, 2011.

Guiot, J., Hai Bin Wu, Wen Ying Jiang, and Yun Li Luo: East Asian Monsoon and paleoclimatic data analysis: a vegetation point of view, Clim. Past, 4, 137–145, doi:10.5194/cp-4-137-2008, 2008.

Hewitt, C. D. and Mitchell, J. F. B.: A fully coupled GCM simulation of the climate of the mid-Holocene, Geophys. Res. Lett., 25, 361–364, 1998.

Holland, M. M., Bailey, D. A., Briegleb, B. P., Light, B., and Hunke, E.: Improved sea ice shortwave radiation physics in CCSM4: the impact of melt ponds and aerosols on Arctic sea ice, J. Climate, 25, 1413–1430, 2012.

CPD
9, 75–118, 2013

Hunke, E. C. and Lipscomb, W. H.: CICE: the Los Alamos sea ice model, documentation and software, version 4.0, Los Alamos National Laboratory Tech. Rep. LA-CC-06-012, 76 pp., 2008.

Jansen, E., Overpeck, J., Briffa, K. R., Duplessy, J.-C., Joos, F., Masson-Delmotte, V., Olago, D., Otto-Bliesner, B., Peltier, W. R., Rahmstorf, S., Ramesh, R., Raynaud, D., Rind, D., Solomina, O., Villalba, R., and Zhang, D.: Palaeoclimate, in: Climate Change 2007: The Physical Science Basis, edited by: Solomon S., Qin, D., Manning, M., Chen, Z., Marquis, M., Averyt, K. B., Tignor, M., and Miller, H. L., Cambridge University Press, 434–497, 2007.

Jiang, D., Lang, X., Tian, Z., and Wang, T.: Considerable model–data mismatch in temperature over China during the mid-Holocene: results of PMIP simulations, J. Climate, 25, 4135–4153, 2012.

Jiang, D., Tian, Z., Lang, X., and Ju, L.: Mid-Holocene net precipitation changes over China: model–data comparison, Quaternary Sci. Rev., submitted, 2013.

Jiang, W., Guiot, J., Chu, G., Wu, H., Yuan, B., Hatté, C., and Guo, Z.: An improved methodology of the modern analogues technique for palaeoclimate reconstruction in arid and semi-arid regions, Boreas, 39, 145–153, 2010.

Joussaume, S., Taylor, K. E., Braconnot, P., Mitchell, J. F. B., Kutzbach, J. E., Harrison, S. P., Prentice, I. C., Broccoli, A. J., Abe-Ouchi, A., Bartlein, P. J., Bonfils, C., Dong, B., Guiot, J., Herterich, K., Hewitt, C. D., Jolly, D., Kim, J. W., Kislov, A., Kitoh, A., Loutre, M. F., Masson, V., McAvaney, B., McFarlane, N., Noblet, N. D., Peltier, W. R., Peterschmitt, J. Y., Pollard, D., Rind, D., Royer, J. F., Schlesinger, M. E., Syktus, J., Thompson, S., Valdes, P., Vettoretti, G., Webb, R. S., and Wyputta, U.: Monsoon changes for 6000 yr ago: results of 18 simulations from the Paleoclimate Modeling Intercomparison Project (PMIP), Geophys. Res. Lett., 26, 859–862, 1999.

Kong, Z. C., Du, N. Q., Shan, F. S., Tong, G. B., Luo, S. J., and Fan, S. X.: Vegetational and climatic changes in the last 11000 yr in Qinghai Lake–numerical analysis based on palynology in core QH85-14C, Mar. Geol. Quaternary Geol., 10, 79–90, 1990 (in Chinese).

Kong, Z. C., Du, N. Q., Zhang, Y. J., Wang, F. B., Liang, Y. L., and Wang, X. C.: Discovery of Helicia fossil florule and sporo-pollen assemblage of Baohuashan in Jurong County and its climatic and botanic significance, Quaternary Sci., 11, 326–335, 1991 (in Chinese).

Kutzbach, J. E. and Liu, Z.: Response of the African monsoon to orbital forcing and ocean feedbacks in the middle Holocene, Science, 278, 440–443, 1997.

CPD
9, 75–118, 2013

Kutzbach, J. E., Bonan, G., Foley, J., and Harrison, S. P.: Vegetation and soil feedbacks on the response of the African monsoon to orbital forcing in the early to middle Holocene, Nature, 384, 623–626, 1996.
Lawrence, D. M., Oleson, K. W., Flanner, M. G., Fletcher, C. G., Lawrence, P. J., Levis, S., Swenson, S. C., and Bonan, G. B.: The CCSM4 land simulation, 1850–2005: assessment of surface climate and new capabilities, J. Climate, 25, 2240–2260, 2012.
Levis, S., Bonan, G. B., and Bonfils, C.: Soil feedback drives the mid-Holocene North African monsoon northward in fully coupled CCSM2 simulations with a dynamic vegetation model, Clim. Dynam., 23, 791–802, 2004.
Li, Y. F. and Harrison, S. P.: Simulations of the impact of orbital forcing and ocean on the Asian summer monsoon during the Holocene, Global Planet. Change, 60, 505–522, 2008.
Li, Y. F., Harrison, S. P., Zhao, P., and Ju, J. H.: Simulations of the impacts of dynamic vegetation on interannual and interdecadal variability of Asian summer monsoon with modern and mid-Holocene orbital forcings, Global Planet. Change, 66, 235–252, 2009.
Liu, Y., He, J. H., Li, W. L., Chen, L. X., Li, W., and Zhang, B.: MM5 simulations of the China regional climate during the mid-Holocene, Acta Meteorol. Sin., 24, 468–483, 2010.
Liu, Z., Harrison, S. P., Kutzbach, J., and Otto-Bliesner, B.: Global monsoons in the mid-Holocene and oceanic feedback, Clim. Dynam., 22, 157–182, 2004.
Marzin, C. and Braconnot, P.: The role of the ocean feedback on Asian and African monsoon variations at 6 kyr and 9.5 kyr BP, C. R. Geosci., 341, 643–655, 2009.
Neale, R. B., Richter, J. H., Conley, A. J., Park, S., Lauritzen, P. H., Gettelman, A., Williamson, D. L., Rasch, P. J., Vavrus, S. J., Taylor, M. A., Collins, W. D., Zhang, M., and Lin, S.: Description of the NCAR Community Atmosphere Model (CAM 4.0), Tech. Rep. NCAR/TN-485+STR, National Center for Atmospheric Research, Boulder, CO, 194 pp., 2010.
Ni, J., Yu, G., Harrison, S. P., and Prentice, I. C.: Palaeovegetation in China during the late Quaternary: biome reconstructions based on a global scheme of plant functional types, Palaeogeogr. Palaeocl., 289, 44–61, 2010.
O'ishi, R. and Abe-Ouchi, A.: Polar amplification in the mid-Holocene derived from dynamical vegetation change with a GCM, Geophys. Res. Lett., 38, L14702, doi:10.1029/2011GL048001, 2011.
Ohgaito, R. and Abe-Ouchi, A.: The role of ocean thermodynamics and dynamics in Asian summer monsoon changes during the mid-Holocene, Clim. Dynam., 29, 39–50, 2007.

CPD
9, 75–118, 2013

Otto, J., Raddatz, T., and Claussen, M.: Climate variability-induced uncertainty in mid-Holocene atmosphere–ocean–vegetation feedbacks, Geophys. Res. Lett., 36, L23710, doi:10.1029/2009GL041457, 2009a.
Otto, J., Raddatz, T., Claussen, M., Brovkin, V., and Gayler, V.: Separation of atmosphere–ocean–vegetation feedbacks and synergies for mid-Holocene climate, Geophys. Res. Lett., 36, L09701, doi:10.1029/2009GL037482, 2009b.
Shi, Y., Kong, Z., Wang, S., Tang, L., Wang, F., Yao, T., Zhao, X., Zhang, P., and Shi, S.: Mid-Holocene climates and environments in China, Global Planet. Change, 7, 219–233, 1993.
Shields, C. A., Bailey, D. A., Danabasoglu, G., Jochum, M., Kiehl, J. T., Levis, S., and Park, S.: The low-resolution CCSM4, J. Climate, 25, 3993–4014, 2012.
Smith, R., Jones, P., Briegleb, B., Bryan, F., Danabasoglu, G., Dennis, J., Dukowicz, J., Eden, C., Fox-Kemper, B., Gent, P., Hecht, M., Jayne, S., Jochum, M., Large, W., Lindsay, K., Maltrud, M., Norton, N., Peacock, S., Vertenstein, M., and Yeager, S.: The Parallel Ocean Program (POP) reference manual, ocean component of the Community Climate System Model (CCSM), Los Alamos National Laboratory Tech. Rep. LAUR-10-01853, 141 pp., 2010.
Tang, L. Y., Shen, C. M., Liu, K., and Overpeck, J. T.: Changes in South Asian monsoon: New high-resolution paleoclimatic records from Tibet, China, Chinese Sci. Bull., 45, 87–91, 2000.
Texier, D., Noblet, N. D., and Braconnot, P.: Sensitivity of the African and Asian monsoons to mid-Holocene insolation and data-inferred surface changes, J. Climate, 13, 164–181, 2000.
Tian, Z., Jiang, D., Zhang, R., and Sui, Y.: Long-term climate simulation of CCSM4.0 and evaluation of its performance over East Asia and China, Chinese J. Atmos. Sci., 36, 619–632, 2012 (in Chinese).
Voss, R. and Mikolajewicz, U.: The climate of 6000 yr BP in near-equilibrium simulations with a coupled AOGCM, Geophys. Res. Lett., 28, 2213–2216, 2001.
Wang, H. J.: Role of vegetation and soil in the Holocene megathermal climate over China, J. Geophys. Res., 104, 9361–9367, 1999.
Wang, H. J.: The seasonal climate and low frequency oscillation in the simulated mid-Holocene megathermal climate, Adv. Atmos. Sci., 17, 445–457, 2000.
Wang, H. J.: The mid-Holocene climate simulated by a grid-point AGCM coupled with a biome model, Adv. Atmos. Sci., 19, 205–218, 2002.
Wang, T., Wang, H. J., and Jiang, D.: Mid-Holocene East Asian summer climate as simulated by the PMIP2 models, Palaeogeogr. Palaeocl., 288, 93–102, 2010.

CPD
9, 75–118, 2013

Wei, J. F. and Wang, H. J.: A possible role of solar radiation and ocean in the mid-Holocene East Asian monsoon climate, Adv. Atmos. Sci., 21, 1–12, 2004.

Wen, R. L., Xiao, J. L., Chang, Z. G., Zhai, D. Y., Zhou, L., Xu, Q. H., Li, Y. C., and Itoh, S.: Holocene vegetation and climate changes reflected by the pollen record of Hulun Lake, north eastern Inner Mongolia, Quaternary Sci., 30, 1105–1115, 2010 (in Chinese).

Wohlfahrt, J., Harrison, S. P., and Braconnot, P.: Synergistic feedbacks between ocean and vegetation on mid- and high-latitude climates during the mid-Holocene, Clim. Dynam., 22, 223–238, 2004.

Xu, Q. H., Chen, S. Y., Kong, Z. C., and Du, N. Q.: Preliminary discussion of vegetation succession and climatic change since the Holocene in the Baiyangdian Lake district, Acta Phytoecol. Geobotan. Sin., 12, 143–151, 1988 (in Chinese).

Yu, G., Prentice, I. C., Harrison, S. P., and Sun, X.: Pollen-based biome reconstructions for China at 0 and 6000 yr, J. Biogeogr., 25, 1055–1069, 1998.

Yu, G., Chen, X., Ni, J., Cheddadi, R., Guiot, J., Han, H., Harrison, S. P., Huang, C., Ke, M., Kong, Z., Li, S., Li, W., Liew, P., Liu, G., Liu, J., Liu, Q., Liu, K.-B., Prentice, I. C., Qui, W., Ren, G., Song, C., Sugita, S., Sun, X., Tang, L., Van Campo, E., Xia, Y., Xu, Q., Yan, S., Yang, X., Zhao, J., and Zheng, Z.: Palaeovegetation of China: a pollen data-based synthesis for the mid-Holocene and last glacial maximum, J. Biogeogr., 27, 635–664, 2000.

Zhao, Y. and Harrison, S. P.: Mid-Holocene monsoons: A multi-model analysis of the inter-hemispheric differences in the responses to orbital forcing and ocean feedbacks, Clim. Dynam., 39, 1457–1487, 2012.

Zheng, W. and Yu, Y.: The Asian monsoon system of the mid-Holocene simulated by a coupled GCM, Quaternary Sci., 29, 1135–1145, 2009 (in Chinese).

Zheng, Y. Q., Yu, G., Wang, S. M., Xue, B., Zhuo, D. Q., Zeng, X. M., and Liu, H. Q.: Simulation of paleoclimate over East Asia at 6 ka BP and 21 ka BP by a regional climate model, Clim. Dynam., 23, 513–529, 2004.

Zhou, B. and Zhao, P.: Inverse correlation between ancient winter and summer monsoons in East Asia?, Chinese Sci. Bull., 54, 3760–3767, 2009.

CPD
9, 75–118, 2013

Table 1. Boundary conditions used for 0-ka and 6-ka experiments.

	0-ka	6-ka
Solar constant ($W m^{-2}$)	1365	1365
Earth's orbital parameters (Orbit)		
Eccentricity	0.0167724	0.018682
Obliquity (°)	23.446	24.105
Angular precession (°)	102.04	0.87
Atmospheric concentrations of greenhouse gases (GHGs)		
CO_2 (ppmv)	284.5	280
CH_4 (ppbv)	791.6	650
N_2O (ppbv)	275.7	270

CPD
9, 75–118, 2013

Table 2. Summary of experiments.

Experiment	Vegetation Treatment	SST Treatment	Orbit	GHGs	Integration
AOV(0 ka)	dynamic	dynamic	0-ka	0-ka	1651 yr
AOV(6 ka)	dynamic	dynamic	6-ka	6-ka	400 yr
AO(0 ka)	fixed as AOV(0 ka)	dynamic	0-ka	0-ka	800 yr
AO(6 ka)	fixed as AOV(0 ka)	dynamic	6-ka	6-ka	700 yr
A(0 ka)	fixed as AOV(0 ka)	fixed as AO(0 ka)	0-ka	0-ka	30 yr
A(6 ka)	fixed as AOV(0 ka)	fixed as AO(0 ka)	6-ka	6-ka	30 yr

CPD
9, 75–118, 2013

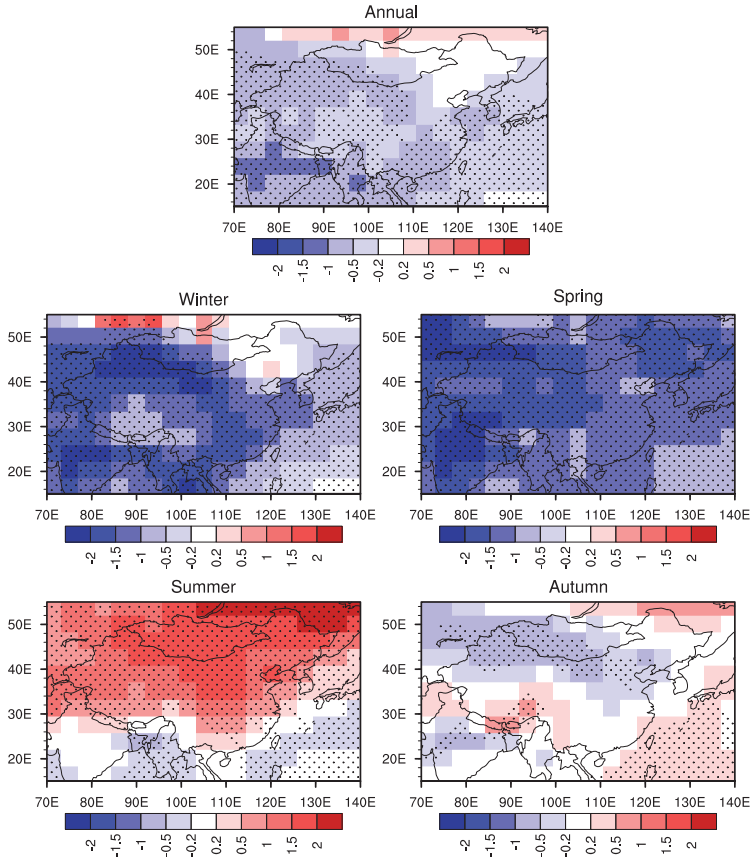

Fig. 1. Annual and seasonal temperature differences (units: K) between AOV(6 ka) and AOV(0 ka) experiments. The areas exceeding 95 % confidence level are dotted.

CPD
9, 75–118, 2013

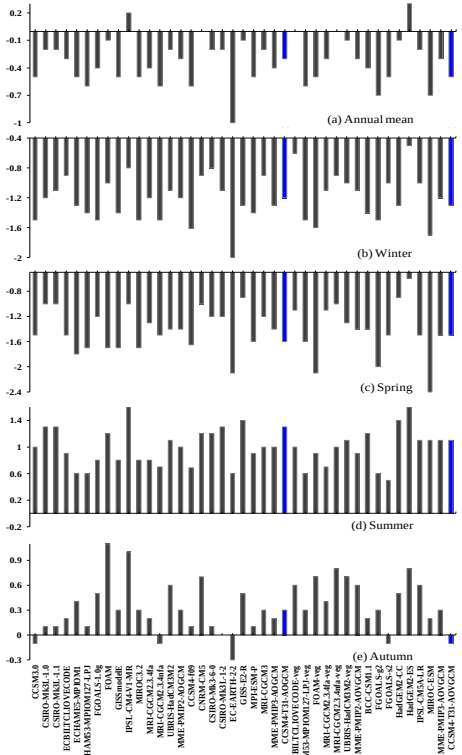

Fig. 2. Mid-Holocene–baseline anomalies of regionally averaged annual and seasonal temperature (units: K) over China. MME-PMIP2-AOGCM denotes the ensemble mean of the 14 PMIP2 AOGCMs; MME-PMIP3-AOGCM denotes the ensemble mean of the eight PMIP3 AOGCMs; MME-PMIP2-AOVGCM denotes the ensemble mean of the six PMIP2 AOVGCMs; MME-PMIP3-AOVGCM denotes the ensemble mean of the seven PMIP3 AOVGCMs; CCSM4-T31-AOGCM and CCSM4-T31-AOVGCM as shown by blue bar stands for the AOGCM and AOVGCM experiments in this study, respectively.

CPD
9, 75–118, 2013

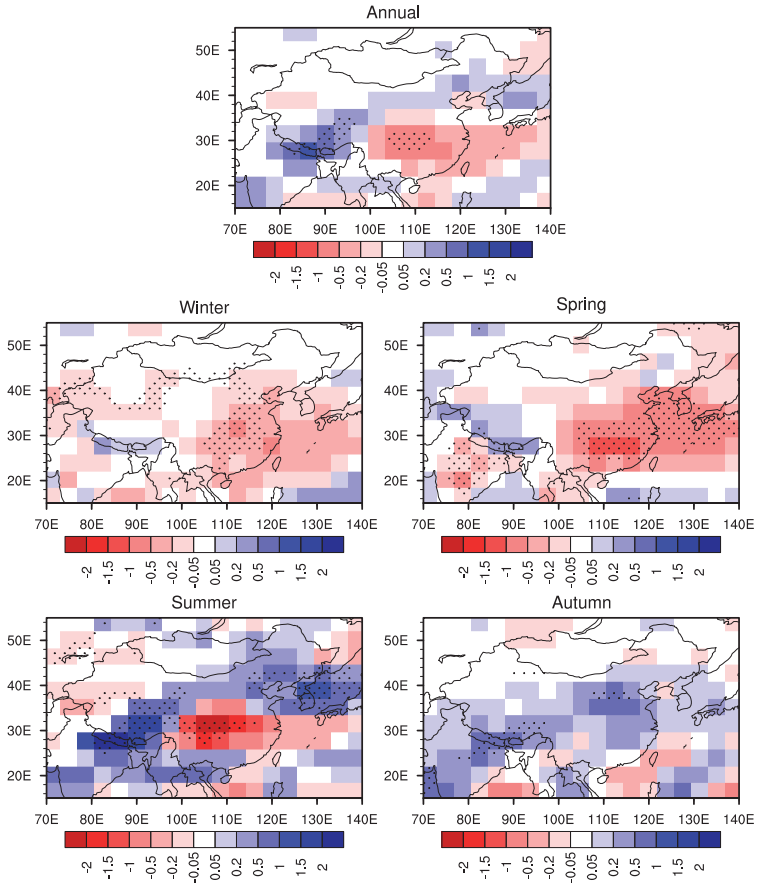

Fig. 3. Same as Fig. 1, but for effective precipitation (precipitation minus evaporation, P–E) changes (units: mm day^{-1}).

CPD
9, 75–118, 2013

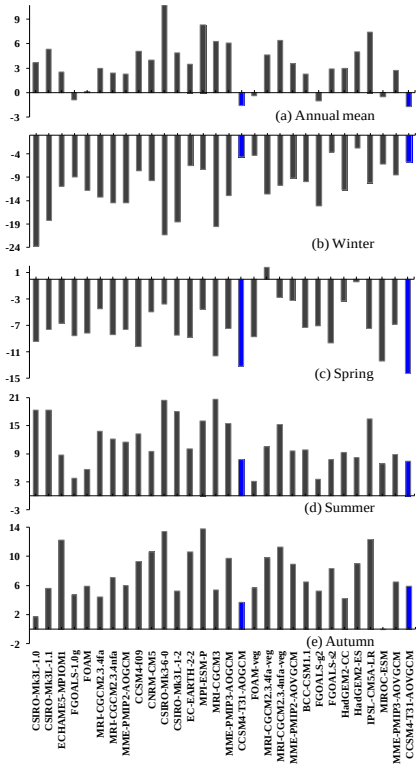

Fig. 4. Percentage change (units: %) of regionally averaged annual and seasonal precipitation over China during the mid-Holocene with respect to the baseline period. MME-PMIP2-AOGCM denotes the ensemble mean of the seven PMIP2 AOGCMs; MME-PMIP3-AOGCM denotes the ensemble mean of the seven PMIP3 AOGCMs; MME-PMIP2-AOVGCM denotes the ensemble mean of the three PMIP2 AOVGCMs; MME-PMIP3-AOVGCM denotes the ensemble mean of the seven PMIP3 AOVGCMs; CCSM4-T31-AOGCM and CCSM4-T31-AOVGCM as shown by blue bar stands for the AOGCM and AOVGCM experiments in this study, respectively.

CPD
9, 75–118, 2013

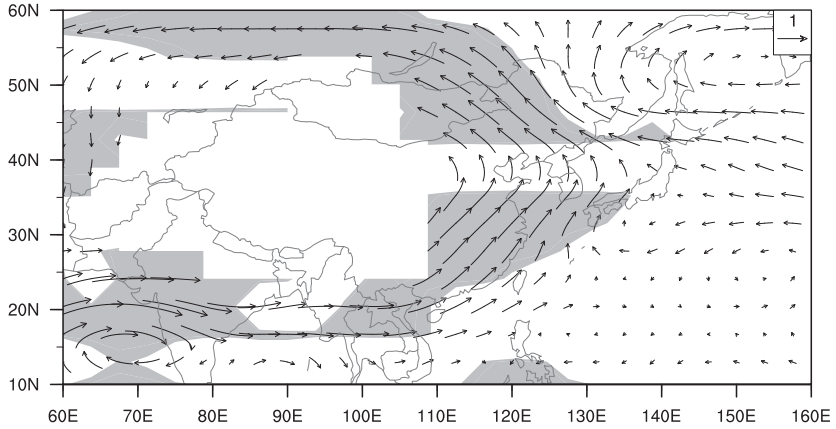

Fig. 5. Mid-Holocene–baseline anomalies of summer wind field at 850 hPa (units: $m s^{-1}$). Regions with an elevation above 1500 m are left blank, and areas exceeding 95 % confidence level are shaded.

CPD
9, 75–118, 2013

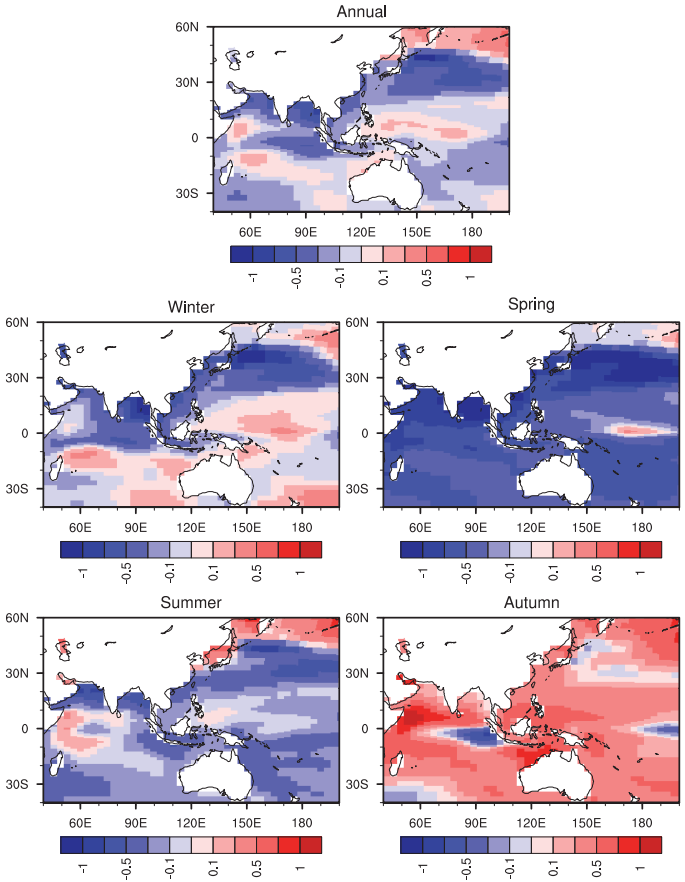

Fig. 6. Simulated differences in annual and seasonal sea surface temperatures (units: K) between the mid-Holocene and pre-industrial period.

CPD
9, 75–118, 2013

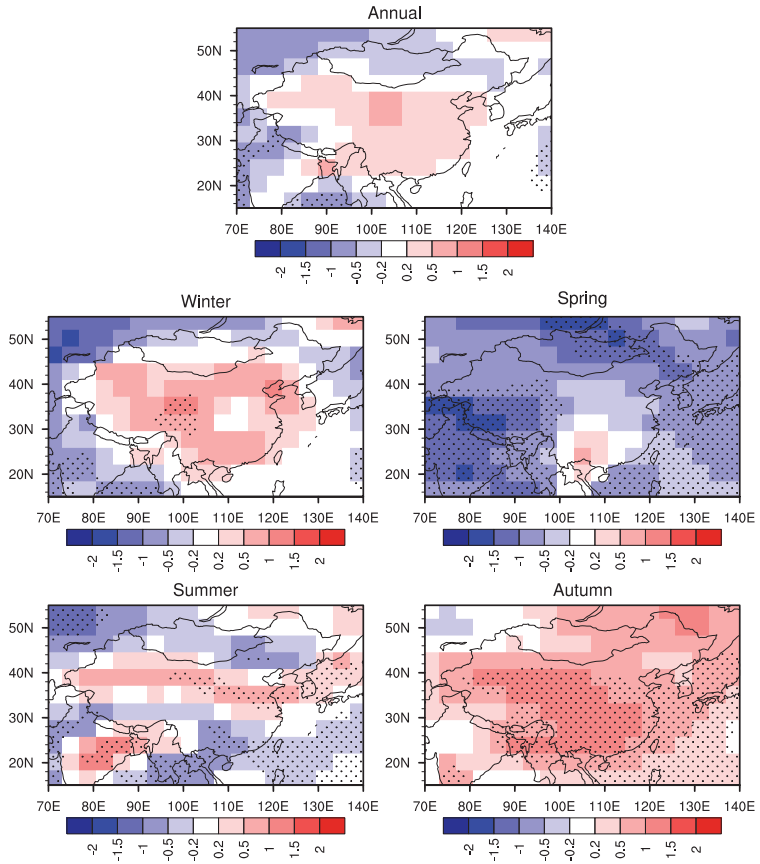

Fig. 7. Annual and seasonal temperature changes (units: K) due to ocean feedback. The areas exceeding 90 % confidence level are dotted.

CPD
9, 75–118, 2013

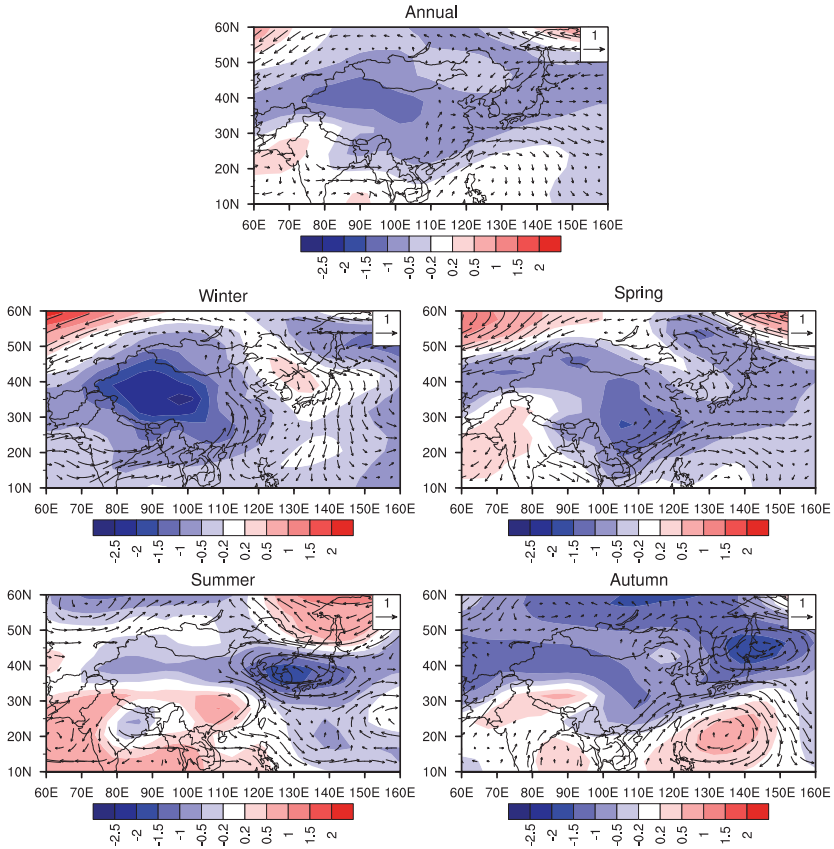

Fig. 8. Annual and seasonal sea level pressure (shaded, units: hPa) and 850 hPa wind (vector, units: $m\,s^{-1}$) changes due to ocean feedback. Wind fields with an elevation above 1500 m are left blank.

CPD
9, 75–118, 2013

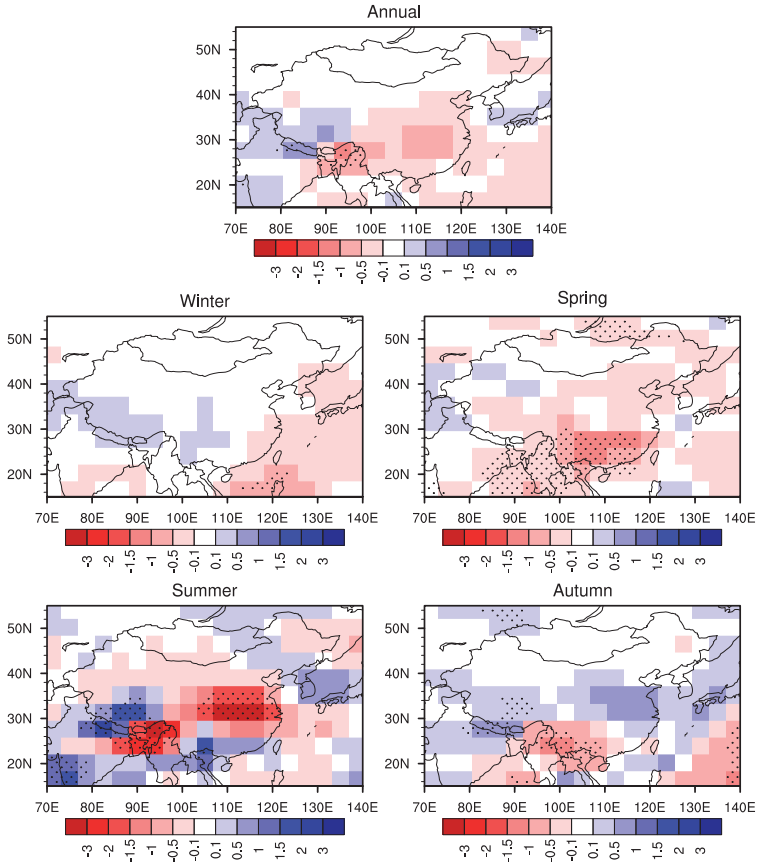

Fig. 9. Annual and seasonal precipitation changes (units: mm day^{-1}) due to ocean feedback. The areas exceeding 90 % confidence level are dotted.

CPD
9, 75–118, 2013

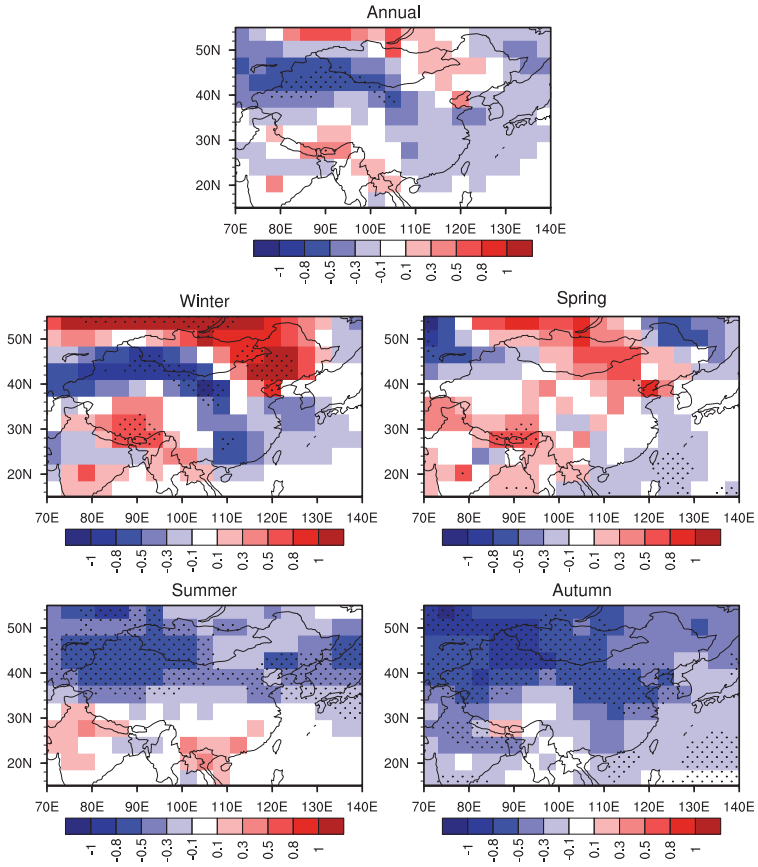

Fig. 10. Annual and seasonal temperature changes (units: K) due to vegetation feedback. The areas exceeding 90 % confidence level are dotted.

CPD
9, 75–118, 2013

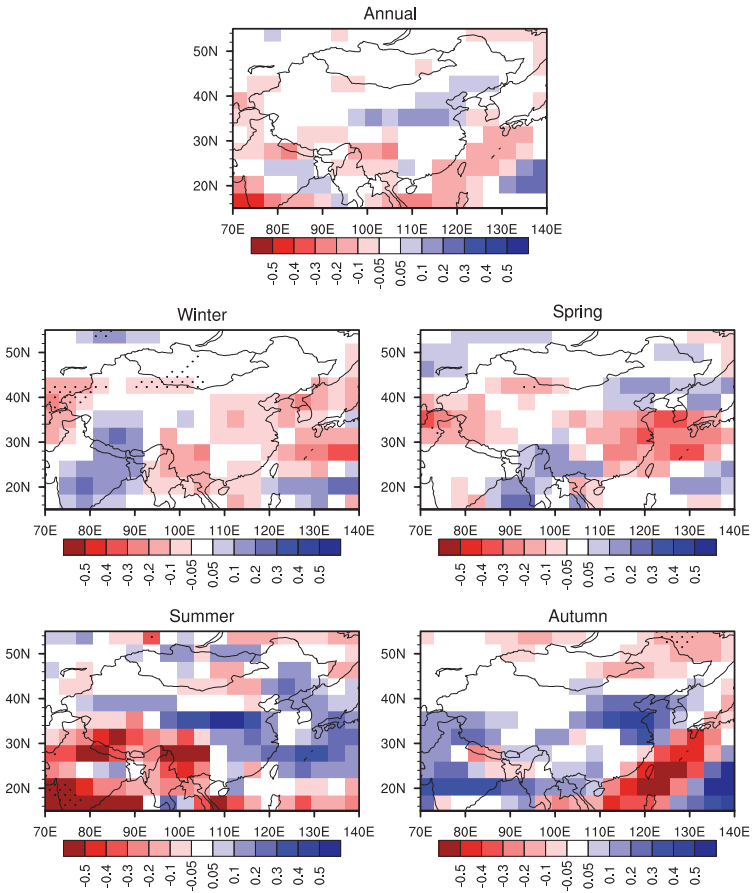

Fig. 11. Annual and seasonal precipitation changes (units: mm day^{-1}) due to vegetation feedback. The areas exceeding 90 % confidence level are dotted.

CPD
9, 75–118, 2013

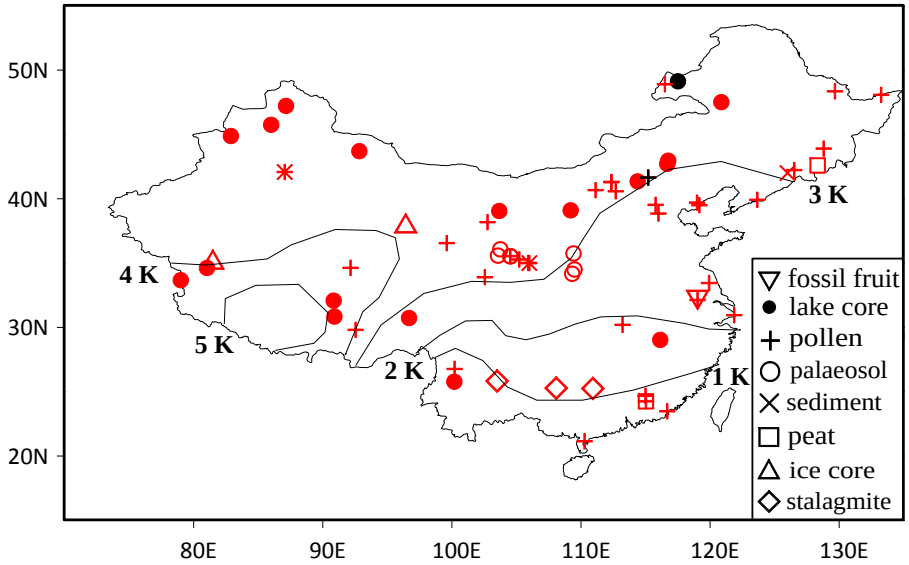

Fig. 12. Proxy estimates of annual temperature changes during the mid-Holocene relative to the present day, cited from Jiang et al. (2012). Red and black symbols represent warmer and normal conditions, and the contours are modified from Shi et al. (1993).

CPD
9, 75–118, 2013